






RESEARCH ARTICLE

Porphyromonas gingivalis impairs glucose uptake in skeletal muscle associated with altering gut microbiota

Kazuki Watanabe¹  | Sayaka Katagiri¹  | Hirokazu Takahashi^{2,3} | Naoki Sasaki¹ | Shogo Maekawa¹ | Rina Komazaki¹ | Masahiro Hatasa¹ | Yoichiro Kitajima^{2,4} | Yusuke Maruyama⁵ | Takahiko Shiba¹ | Keiji Komatsu¹ | Yujin Ohsugi¹ | Kenichi Tanaka² | Ayumi Matsuzawa⁶ | Tomomitsu Hirota⁷ | Haruka Tohara⁸  | Yuichiro Eguchi³ | Keizo Anzai² | Atsuhiko Hattori⁵  | Takanori Iwata¹ 

¹Department of Periodontology, Graduate School of Medical and Dental Sciences, Tokyo Medical and Dental University (TMDU), Tokyo, Japan

²Division of Metabolism and Endocrinology, Faculty of Medicine, Saga University, Saga, Japan

³Liver Center, Saga University Hospital, Saga University, Saga, Japan

⁴Department of Radiology, Eguchi Hospital, Saga, Japan

⁵Department of Biology, College of Liberal Arts and Sciences, Tokyo Medical and Dental University (TMDU), Tokyo, Japan

⁶Department of Epigenetics, Medical Research Institute, Tokyo Medical and Dental University (TMDU), Tokyo, Japan

⁷Division of Molecular Genetics, Research Center for Medical Science, The Jikei University School of Medicine, Tokyo, Japan

⁸Dysphagia Rehabilitation, Department of Gerontology and Gerodontology, Graduate School of Medical and Dental Sciences, Tokyo Medical and Dental University (TMDU), Tokyo, Japan

Correspondence

Sayaka Katagiri, Department of Periodontology, Graduate School of Medical and Dental Sciences, Tokyo Medical and Dental University, 1-5-45 Yushima, Bunkyo-ku, Tokyo 1138510, Japan.

Email address: katagiri.peri@tmd.ac.jp

Hirokazu Takahashi, Division of Metabolism and Endocrinology, Faculty of Medicine, Saga University, 5-1-1 Nabeshima, Saga 8498501, Japan. Email: takahas2@cc.saga-u.ac.jp

Funding information

MEXT | Japan Society for the Promotion of Science (JSPS), Grant/Award Number: JP17K11982, JP18K15754, JP19K24062, JP19K18989, JP19K10221, JP18K11016, JP20J13034 and JP20H03863

Abstract

Skeletal muscles have a high metabolic capacity, which play key roles in glucose metabolism. Although periodontal disease increases the risk of metabolic syndrome, the relationship between periodontal bacterial infection and skeletal muscle metabolic dysfunction is unclear. We found that anti-*Porphyromonas gingivalis* (*Pg*) antibody titers positively correlated with intramuscular adipose tissue content (IMAC), fasting blood glucose, and HOMA-IR in metabolic syndrome patients. In C57BL/6J mice fed a high-fat diet, recipients of oral *Pg* (HFPg) had impaired glucose tolerance, insulin resistance, and higher IMAC compared to recipients of saline (HFco). The soleus muscle in HFPg mice exhibited fat infiltration and lower glucose uptake with higher *Tnfa* expression and lower insulin signaling than in HFco mice. Gene set enrichment analysis showed that TNF α signaling via NF κ B gene set was enriched in the soleus muscle of HFPg mice. Moreover, TNF- α also decreased glucose uptake in C2C12 myoblast cells in vitro.

Abbreviations: 2DG, 2-deoxyglucose; 2DG6P, 2DG-6-phosphate; ALP, alkaline phosphatase; ALT, alanine aminotransferase; ANCOM, analysis of composition of microbiomes; ANOSIM, analysis of similarities; AST, aspartate aminotransferase; BMI, body mass index; CFU, colony forming units; FDR, false discovery rate; GSEA, gene set enrichment analysis; HOMA-IR, homeostasis model of assessment of insulin resistance; IMAC, intramuscular adipose tissue content; LC, liquid chromatography; MS, metabolic syndrome; *Pg*, *Porphyromonas gingivalis*; QIIME 2, quantitative insights into microbial ecology 2; SAI, skeletal muscle area index; γ -GTP, γ -glutamyl transpeptidase.

Based on 16S rRNA sequencing, *Pg* administration altered the gut microbiome, particularly by decreasing the abundance of genus *Turicibacter*. Microbial network of the gut microbiome was dramatically changed by *Pg* administration. Our findings suggest that infection with *Pg* is a risk factor for metabolic syndrome and skeletal muscle metabolic dysfunction via gut microbiome alteration.

KEYWORDS

glucose uptake, metabolic syndrome, periodontal disease, *Porphyromonas gingivalis*, skeletal muscle

1 | INTRODUCTION

Skeletal muscles, the most representative tissues in the body, are essential for voluntary movement and postural position.¹ In addition, skeletal muscles play important roles in nutritional balance, thermal regulation, endocrine system regulation, energy metabolism, and glucose uptake.^{2,3} Approximately one-quarter of all ingested glucose is stored as glycogen in skeletal muscles for use as an energy source.⁴

The clinical consequences of insulin resistance and compensatory hyperinsulinemia have become a major public health problem.⁵ Insulin resistance plays a crucial role in the pathogenesis of insulin resistance syndrome, alternatively named “metabolic syndrome” (MS).⁶ MS manifests with various clinical features, including obesity, atherogenic dyslipidemia, elevated blood pressure, elevated plasma glucose, and a pro-inflammatory state. Furthermore, MS drastically increases the risk of type 2 diabetes mellitus.⁷

Periodontal disease is characterized by the destruction of the alveolar bone and connective tissues caused by pathogenic oral microorganisms.⁸ Periodontal bacteria present in dental plaques express virulence factors, including lipopolysaccharide, fimbriae, and enzymes, which can induce inflammation.^{8,9} A relationship between MS and periodontal disease has been established.¹⁰ Periodontal disease increases the risks of obesity,¹¹ diabetes mellitus,¹² and MS.¹³ We previously reported that infection with periodontal bacteria increased body weight and insulin resistance in mice by altering their gut microbiome.¹⁴

However, the relationship between periodontal bacterial infection and metabolic impairment in skeletal muscles is unclear. Therefore, the present study aimed to clarify the relationship between periodontal disease and MS. We measured the titers of IgG antibodies against periodontopathic bacteria in MS patients. We then investigated the influence of *Porphyromonas gingivalis* (*Pg*) infection on glucose metabolism, the gut microbiota, steatosis, and glucose uptake in murine skeletal muscle.

2 | MATERIALS AND METHODS

2.1 | Patients

We enrolled 35 Japanese patients admitted to the Eguchi Hospital and Saga Medical School for the treatment of MS. MS was identified according to the Japanese diagnostic criteria.¹⁵ MS was diagnosed based on waist circumference (as a measure of central obesity) ≥ 85 cm for men and ≥ 90 cm for women and/or a visceral fat area ≥ 100 cm². In addition, the patients had to fulfill two or more of the following criteria: (1) triglyceride levels ≥ 150 mg/dL and HDL-cholesterol ≤ 40 mg/dL; (2) blood pressure: systolic ≥ 130 mm Hg and diastolic ≥ 85 mm Hg; and (3) fasting blood glucose level ≥ 110 mg/dL. Patient body mass index was calculated as the body weight in kilograms divided by the square of the height in meters (kg/m²). Venous blood samples were acquired from all subjects at approximately 9:00 AM, following a 12-h overnight fast to measure plasma glucose (mg/dL). Serum from the patients' venous blood was collected using vacuum blood collection tubes containing EDTA and stored at -80°C before analyzing IgG antibody titers.

We performed abdominal computed tomography (CT) with unenhanced spiral acquisition to calculate intramuscular adipose tissue content (IMAC) in the lumbar muscles, as described previously.¹⁶ The study was performed in accordance with the Ethical Guidelines for Clinical Studies. All patients provided informed consent, and the study protocol was approved by the ethics committees of Saga University (2018-12-13) and Tokyo Medical and Dental University (D2019-001).

2.2 | Serum IgG titer measurement

Specific serum IgG titers were measured by enzyme-linked immunosorbent assay, as described previously,^{14,17} using sonicated whole-cell extracts of the individual periodontal bacteria. Briefly, 96-well microplates were coated with sonicated *Pg* ATCC 33277, *Aggregatibacter actinomycetemcomitans* (*Aa*) ATCC 43718, or *Fusobacterium nucleatum* (*Fn*) (10 $\mu\text{g}/\text{mL}$ in carbonate buffer). Serially diluted positive control reference serum (2^5 - 2^{15} dilution, 200 μL per well) and singly diluted patient serum (2^{10} dilution, 200 μL per well) were added to each well. Subsequently, alkaline phosphatase-conjugated goat antihuman IgG (200 μL per well; Sigma-Aldrich) was added. Following incubation, the plates were washed and developed with a phosphatase substrate (Sigma-Aldrich). We read the optical density at 450 nm using a microplate reader (SoftMax, Molecular Devices, Sunnyvale, CA, USA).

2.3 | Cultivation of *Pg*

Pg was cultivated as previously described.^{17,18} Briefly, the bacteria were maintained on trypticase soy agar supplemented with 10% of defibrinated horse blood, hemin, and menadione at 37°C under anaerobic conditions. After 48 hours of incubation, *Pg* was inoculated into trypticase soy broth under anaerobic conditions.

2.4 | Animals

C57BL/6J mice (8 weeks old; Sankyo Laboratory, Tokyo, Japan) were used in this study. Mice were randomly assigned into four groups: NCco, NCPg, HFco, and HFPg. HFco and HFPg mice were fed high-fat diet 32 (CLEA Japan, Tokyo, Japan). We orally administered 10⁸ CFU sonicated *Pg* in 100 µL of saline to mice in the NCPg and HFPg groups and saline only to mice in the NCco and HFco. The suspension was given twice per week for 6 weeks. Glucose tolerance test and insulin tolerance test were performed as previously described.^{14,19} Briefly, after fasting for 6 hours, mice were fed glucose by oral gavage (1 g/kg) or were given an intraperitoneal injection of insulin (1 U/kg) (Humulin R; Eli Lilly and Company, Indianapolis, IN, USA). Glucose concentration was determined with a glucose meter (ACCU-CHEK ST Meter; Roche, Basel, Switzerland). The area under the curve (AUC) (0-120 minutes) was calculated for each mice group. Soleus and tibialis anterior muscles were collected after 6 hours of fasting to evaluate gene expression and steatosis. To evaluate insulin signaling in the muscles, mice were fasted for 6 hours, then, injected with insulin (1 U/kg body weight). Muscles were collected 10 minutes after insulin injection and stored at -80°C. To evaluate glucose uptake in the muscles, we injected the mice with insulin (1 U/kg body weight), then, injected 2-deoxyglucose (2DG; Sigma-Aldrich, St. Louis, MO, USA) (200 mg/kg body weight) 15 minutes later. Muscles were collected 15 minutes after 2DG injection and stored at -80°C until 2DG-6-phosphate (2DG6P) measurement. All protocols concerning animal use and euthanasia were reviewed and approved by the Animal Care Committee of the Experimental Animal Center at Tokyo Medical and Dental University (A2019-084C2).

2.5 | CT analysis of the lumbar muscle in mice

Micro-CT imaging was performed on mice anesthetized with isoflurane with a micro-CT unit (RmCT2; Rigaku Corporation, Tokyo, Japan). We calculated the IMAC as described in the Patients section.¹⁶ The skeletal muscle area index (SAI) was calculated as the abdominal lumbar muscle

area divided by the square of the length from the base of tail to the head in meters (cm²/m²) to adjust for size differences.¹⁶

2.6 | Triglyceride and glycogen measurement

Triglycerides and glycogen were measured, as previously described.¹⁸ Muscle triglycerides were estimated by measuring glycerol with optical density measurement at 540 nm. Glycogen content was expressed as glucose units in the skeletal muscle.²⁰ Muscles were hydrolyzed, and glycogen concentrations were determined by the hexokinase enzymatic method; the optical density value was measured at 340 nm.

2.7 | Histological analysis of skeletal muscle

Samples were fixed in 4% of paraformaldehyde in PBS at 4°C for 24 hours, then, placed to sucrose buffer at 4°C. Tissues were embedded in an OCT compound and stained with Oil Red O. The adipocyte cross-sectional area was measured using Adobe Photoshop CC Software (Adobe Systems, San Jose, CA, USA).

2.8 | Measurement of 2DG6P

Muscle tissues were homogenized in ultrapure water, then, centrifuged, and supernatants were collected. To measure 2DG6P levels, we used an LC-MS-8050 triple quadrupole liquid chromatograph mass spectrometer (Shimadzu, Kyoto, Japan) coupled to an LC-30AD high-performance liquid chromatograph (Shimadzu) and an SIL-30AC (Shimadzu). An amide-80 column (Tosoh Bioscience, King of Prussia, PA, USA) was used with a column oven temperature of 25°C. The isocratic elution consisted of 10 mM ammonium acetate with 0.05% of acetic acid and methanol (3:1, v/v), and the flow rate was 0.4 mL/min. The quantification was performed using a mass spectrometer equipped with an electrospray ionization source in multiple reaction monitoring mode. 2DG6P was monitored in positive ionization mode using transitions of m/z 243.15 → m/z 96.75. To confirm the compounds, we also monitored at the transition of m/z 243.15 → m/z 78.90. LC solution software (Shimadzu) was used for instrument control and data acquisition.

2.9 | Skeletal muscle lysate preparation and western blotting

Lysates from frozen muscles were extracted with sodium dodecyl sulfate sample buffer, then, cleared and used for western

blotting. Antibodies against Erk, pErk, Akt, and pAkt were purchased from Cell Signaling Technology (Danvers, MA, USA), and goat anti-rabbit IgG was purchased from Santa Cruz Biotechnology (Santa Cruz, CA, USA).

2.10 | RNA preparation and quantitative polymerase chain reaction

Extraction of total RNA from the muscles and quantitative polymerase chain reaction (qPCR) were performed as previously described.¹⁴ Gene expression levels were normalized to those of the reference gene, *18S ribosomal* RNA. qPCR amplification was carried out using a Thermal Cycler Dice® Real-Time System II (TaKaRa Bio) and SYBR Ex *Taq* DNA Polymerase II (Takara Bio). Each sample was measured in duplicate. The amplification conditions comprised 40 cycles of denaturation at 95°C for 10 seconds and annealing/extension at 56°C for 30 seconds followed by melting curve analysis. The PCR primers used in the study are listed in Table 1.

2.11 | Microarray and data analysis

cRNA was generated from 200 ng total RNA, then, hybridized onto an Agilent SurePrint G3 Unrestricted Gene Expression 8 × 60K Microarray (Agilent Technologies, Santa Clara, CA, USA), as described previously (18). Fluorescence signals from the hybridized microarrays were detected using the Agilent Microarray Scanner System (Agilent). The raw microarray data were extracted using Feature Extraction Software (ver. 11.0.1.1; Agilent).

2.12 | Cell culture

C2C12 myoblast cells were cultured in Dulbecco's modified Eagle's medium (DMEM, Gibco, Waltham, MA, USA) supplemented with 10% of heat-inactivated fetal bovine serum (Gibco) at 37°C with 5% of CO₂ in a humidified incubator. C2C12 cells were seeded at a density of 1 × 10⁴ cells/mL/well in 24-well plates and cultured for 24 hours, then, serum-starved for 3 hours by replacing the medium with glucose-free DMEM (Gibco). Then, cells were preincubated with TNF-α, and 2DG (1 mM) was added for 30 minutes. Collected cells were sonicated and centrifuged. The supernatants were stored at -80°C until 2DG6P measurement.

2.13 | 16S rRNA gene sequencing and illumina sequence data processing

DNA extraction from mouse feces, purification, and generation of the multiplexed amplicon library (16S rDNA V3-V4 region) were performed, and the sequences were obtained as previously described.^{14,18} The sequence data are available in the DNA Data Bank of Japan (accession number: DRA009700 for mice fed a high-fat diet and DRA010865 for mice fed a normal diet). The sequence data were processed and analyzed using the QIIME 2²¹ (version 2019.7) custom pipeline. Taxonomic classification of amplicon sequence variants was performed using QIIME feature-classifier classify-sklearn based on Greengenes 13.8 at 99% sequence similarity. Differential abundance between groups at each taxonomic level was tested using analysis of composition of microbiomes (ANCOM).²² Co-occurrence coefficients of the genus level were calculated using the SparCC

TABLE 1 Primers used for quantitative PCR analysis

Gene	Primers	
	Forward (5'-3')	Reverse (5'-3')
<i>Tnfa</i>	ACGGCATGGATCTCAAAGAC	AGATAGCAAATCGGCTGACG
<i>Il6</i>	TAGTCCTTCTACCCCAATTTCC	TTGGTCCTTAGCCACTCCTTC
<i>Ccl2</i>	GACTGCTGCCTGGGTTACC	TGGCGGAAGTAGAATCTCACA
<i>Ppargc1b</i>	TCCTGTAAAAGCCCGGAGTAT	GCTCTGGTAGGGGACAGTGA
<i>Glut1</i>	GCTTCTCCAACCTGGACCTCAAAC	ACGAGGAGCACCGTGAAGATGA
<i>Glut4</i>	ACCGGCAGCCTCTGATCATCG	AGCCGACTCGAAGATGCTGGTTG
<i>Acc2</i>	CGCTCACCAACAGTAAGGTGG	GCTTGGCAGGGAGTTCCTC
<i>Myod1</i>	ATGATGACCCGTGTTTCGACT	CACCGCAGTAGGGAAGTGT
<i>Myf5</i>	AGGAAAAGAAGCCCTGAAGC	GCAAAAAGAAGCAGGCAGAGG
<i>Myog</i>	TGTGTCCGTGGACCGGAGGA	CCGCTGGTTGGGGTTGAGCA
<i>Foxo1</i>	CCCAGGCCGGAGTTTAACC	GTTGCTCATAAAGTCGGTGCT
<i>Il4</i>	GGTCTCAACCCCGAGCTAGT	GCCGATGATCTCTCTCAAGTGAT
<i>18S</i>	GTAACCCGTTGAACCCCAT	CCATCCAATCGCTAGTAGCG

TABLE 2 Characteristics of the patients with MS

	All patients n = 35	Males n = 22	Females n = 13
Age (years)	52 ± 14.1	45 ± 15.1	60 ± 8.2
weight (kg)	70 ± 12.4	76 ± 11.4	60 ± 6.9
BMI (kg/m ²)	27 ± 3.1	27 ± 3.4	26 ± 2.5
AST (IU/L)	27 ± 10.0	29 ± 10.0	23 ± 9.0
ALT (IU/L)	34 ± 20.0	39 ± 20.0	25 ± 16.4
ALP (IU/L)	231 ± 73.4	208 ± 70.0	274 ± 62.0
γ-GTP (IU/L)	68 ± 88.0	88 ± 103.4	31 ± 21.5
Fasting blood glucose (mg/dL)	105 ± 15.7	106 ± 17.4	102 ± 12.6
HOMA-IR	2.0 ± 1.6	2.0 ± 1.1	2.0 ± 2.1
Total cholesterol (mg/dL)	276 ± 144.5	289 ± 112.1	258 ± 202.4

Note: Data are shown as mean ± standard deviation.

program.²³ The parameters for this analysis were as previously described except for SparCC values.²⁴ The networks were visualized using Cytoscape software v.2.8.

2.14 | Statistical analysis

Data distribution was assessed using the Shapiro-Wilk test. Correlation between anti-periodontal bacteria IgG antibody titers and clinical/biochemical parameters was evaluated by Spearman's rank correlation coefficient. In animal experiments, Student's t test was applied to compare two groups. Multiple comparisons in vitro were evaluated using Dunnett's multiple comparison test. Microarray data were quantile-normalized, log₂-transformed, and analyzed as described previously.^{18,25} Assessment of significantly different taxa between different treatment groups was performed using the ANCOM program in QIIME 2. When the requirement of using ANCOM (less than 25% of features are changing between groups) was not fulfilled, statistical significance was calculated using the Benjamin and Hochberg's false discovery rate (FDR) to account for multiple testing. Analysis of similarities (ANOSIM) was used to evaluate the significance of dissimilarity between two groups by applying a dissimilarity matrix value of 1-Pearson coefficient.

3 | RESULTS

3.1 | Correlation between anti-periodontal pathogen IgG antibody titers and the clinical/biochemical parameters of MS patients

The clinical and biochemical characteristics of the subjects enrolled in this study are summarized in Table 2. We

evaluated the correlation between the titers of IgG antibodies against three major periodontopathic bacteria—*Pg*, *Aa*, and *Fn*—and the clinical and biochemical parameters of patients with MS. The anti-*Pg* IgG antibody titers positively correlated with IMAC as evaluated by abdominal CT scans (Figure 1A; $P = .0022$, $\rho = 0.41$), whereas anti-*Aa* and anti-*Fn* IgG antibody titers did not (Figure 1B,C). Anti-*Pg* and anti-*Aa* IgG antibody titers positively correlated with fasting blood glucose levels (Figure 1D,E; anti-*Pg*: $P = .035$ and $\rho = 0.21$; anti-*Aa*: $P = .0050$ and $\rho = 0.35$) and the homeostasis model of assessment of insulin resistance (HOMA-IR; Figure 1G,H; anti-*Pg*: $P = .017$ and $\rho = 0.27$; anti-*Aa*: $P = .020$, $\rho = 0.25$). In contrast, no such correlations were observed between anti-*Fn* IgG antibody titers and fasting blood glucose levels (Figure 1F) or HOMA-IR (Figure 1I).

3.2 | *Pg* administration-induced impaired glucose tolerance, insulin resistance, and fat infiltration in murine skeletal muscle

Based on the significant correlation between *Pg* infection and the IMAC, we investigated if *Pg* affected glucose metabolism and steatosis in murine skeletal muscle. After 6 weeks, HFPg mice had impaired glucose tolerance (Figure 2A) and insulin resistance (Figure 2B) compared HFco mice. We conducted a three-dimensional micro-CT analysis to quantify fat infiltration in the lumbar muscles of the mice. We found that the IMAC was significantly higher and the SAI was significantly lower in the HFPg mice than in the HFco mice (Figure 2C,D). After 6 weeks on the diets, the HFPg mice had significantly higher triglyceride levels in the soleus muscle but not the tibialis anterior muscle than the HFco mice after 6 hours of fasting. The glycogen levels in the soleus and tibialis anterior muscles did not differ between the HFco and HFPg mice (Figure 2F). Histological analysis showed marked lipid accumulation in the soleus muscles of the HFPg mice compared to the HFco mice (Figure 2G-I). However, we did not observe a statistical difference in the lipid area of the tibialis anterior muscle between the HFco and HFPg mice (Figure 2J-L). NCPg mice showed insulin resistance compared to NCco mice. However, IMAC, SAI, triglyceride, and glycogen in the muscle did not differ between NCco and NCPg mice, and no difference in the lipid area of the soleus and tibialis anterior muscles between NCco and NCPg mice was observed (Supporting Information S1).

3.3 | *Pg* administration inhibited glucose uptake in the soleus muscle by altering insulin signaling and gene expression

During intracellular metabolism, 2DG, a glucose molecule in which the 2-hydroxyl group is replaced with hydrogen, is

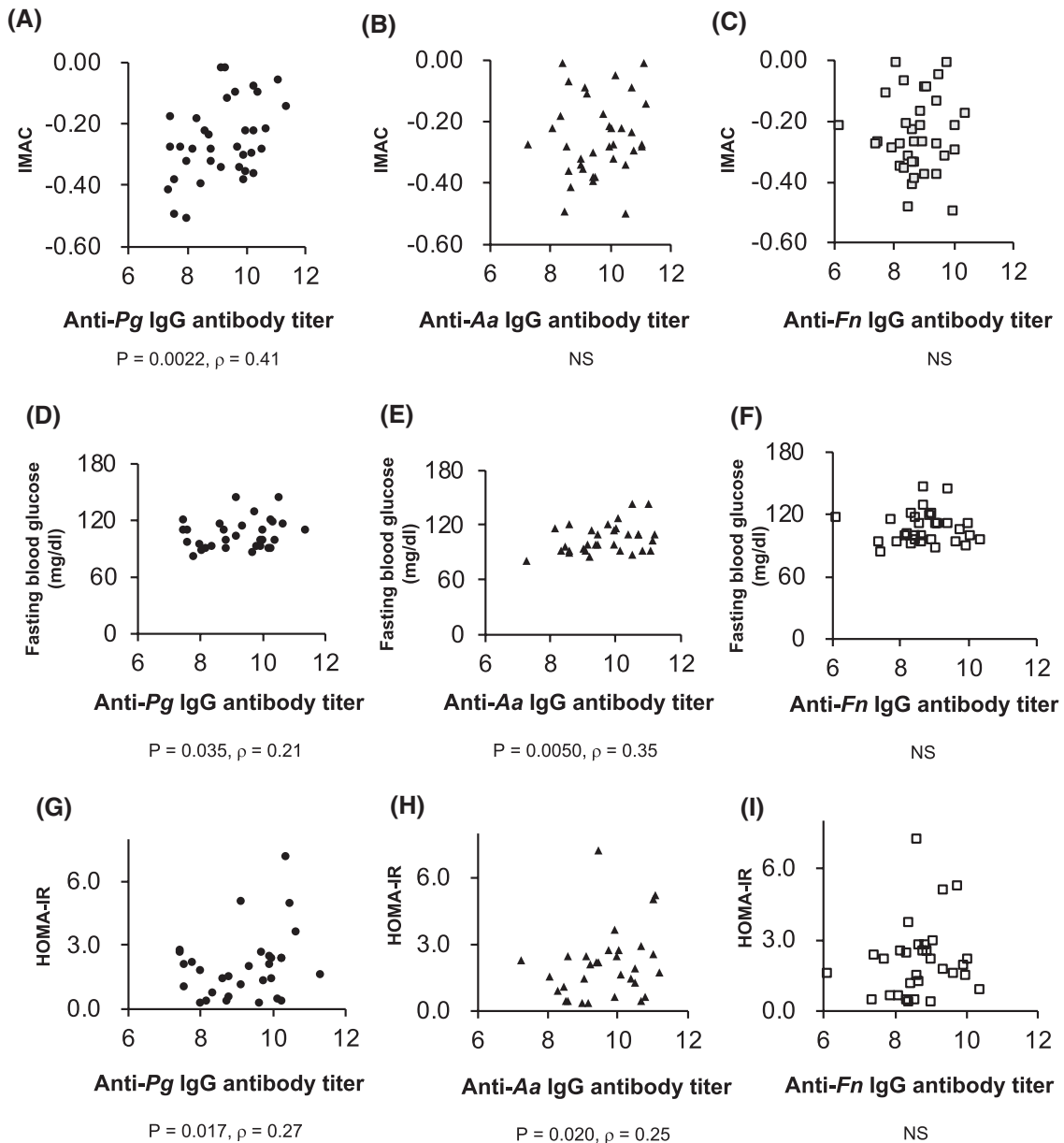


FIGURE 1 Correlations between IgG antibody titers to periodontal pathogen and clinical/biochemical parameters in MS patients ($n = 35$). Correlation between intramuscular adipose tissue content (IMAC) and (A) anti-*Pg* IgG antibody titer, (B) anti-*Aa* IgG antibody titer, (C) anti-*Fn* IgG antibody titer. Correlation between fasting blood glucose and (D) anti-*Pg* IgG antibody titer, (E) anti-*Aa* IgG antibody titer, (F) anti-*Fn* IgG antibody titer. Correlation between HOMA-IR and (G) anti-*Pg* IgG antibody titer, (H) anti-*Aa* IgG antibody titer, (I) anti-*Fn* IgG antibody titer

converted to 2DG6P. Since 2DG6P accumulates in cells due to the absence of downstream metabolizing systems,²⁶ glucose uptake can be estimated by measuring 2DG6P levels. Although we did not observe a statistical difference in 2DG uptake by the tibialis anterior muscle in the HFco and HFp mice (Figure 3C), a significantly lower 2DG uptake by the soleus muscle of HFp mice was observed (Figure 3A). The levels of phosphorylated Akt (pAkt) were significantly lower in the soleus muscles of HFp mice than in those of HFco mice, whereas phosphorylated Erk (pErk) levels were significantly higher (Figure 3B). In the tibialis anterior muscle, we observed significantly lower levels of pAkt but not pErk in

HFp mice than in HFco mice (Figure 3D). Oral administration of *Pg* led to higher mRNA expression levels of tumor necrosis factor alpha (*Tnfa*), interleukin-6 (*Il6*), C-C motif chemokine 2 (*Ccl2*), PPARG coactivator 1 beta (*Ppargc1b*), and myogenin (*Myog*), and lower mRNA expression level of forkhead box O1 (*Foxo1*) in the soleus muscle than the administration of saline (Figure 3E). On the contrary, the mRNA expression levels of *Tnfa*, *Ccl2*, *Ppargc1b*, glucose transporter 4 (*Glut4*), acetyl-CoA carboxylase (*Acc2*), and *Myog* were significantly higher in the tibialis anterior muscles of HFp mice than in those of HFco mice (Figure 3F). Although no significant difference in 2DG uptake in the

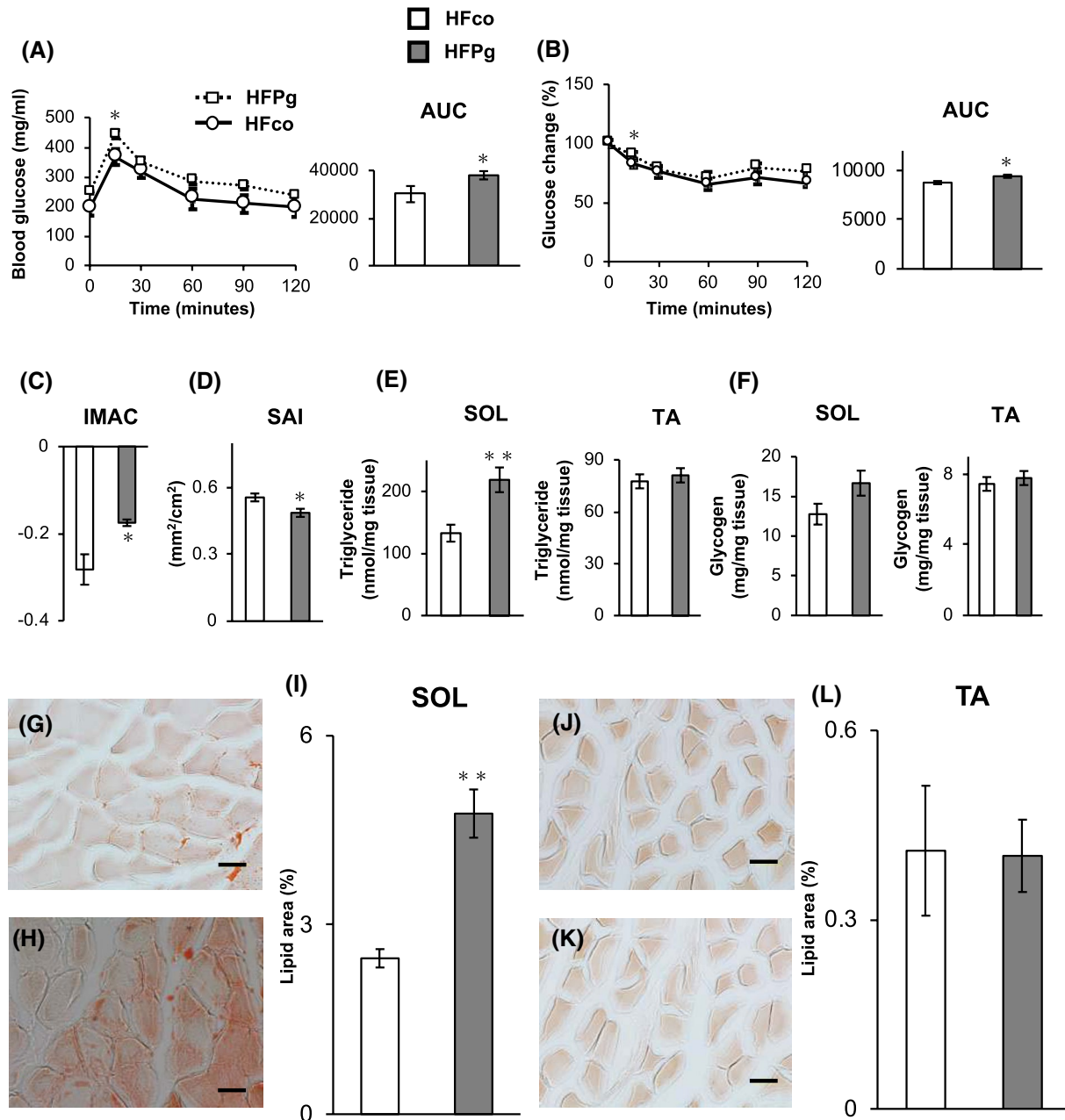


FIGURE 2 Comparison of glucose tolerance, insulin resistance, and evaluation of skeletal muscle fat infiltration between HFco and HFPg mice. A, GTT (1 g/kg) and (B) ITT (1 U/kg) performed at 6 weeks after 6 hours fasting ($n = 7-8$). Comparison of (C) intramuscular adipose tissue content (IMAC) and (D) skeletal muscle area index (SAI) between HFco and HFPg mice ($n = 5$). E, Triglyceride and (F) glycogen in the soleus (SOL) and tibialis anterior (TA) muscles in HFco and HFPg mice at 6 weeks after 6 hours fasting ($n = 5$). Oil red O staining ($n = 5$) in SOL from (G) HFco, (H) HFPg mice. I, Lipid area (%) in the soleus muscle. Oil red O staining ($n = 5$) in TA from (J) HFco and (K) HFPg mice. L, Lipid area (%) in the tibialis anterior muscle. Row magnification $\times 400$, black bar = 50 μm . Data are presented as mean \pm standard error. * $P < .05$ and ** $P < .01$

soleus and tibialis anterior muscles between NCco and NCPg mice was observed, the levels of phosphorylation of Akt in the soleus muscle of NCPg mice was significantly lower than in that of NCco mice. *Tnfa* expression was significantly higher in the soleus muscle of NCPg mice than in that of NCco mice (Supporting Information S2). Melting curves in qPCR for the above genes are shown in the Supporting Information S3.

3.4 | Skeletal muscle microarray analysis with or without *Pg* administration

All of the microarray data from this study are available in the Gene Expression Omnibus database (www.ncbi.nlm.nih.gov/geo) as GSE 146635 (soleus muscle) and GSE 146094 (tibialis anterior muscle). In the soleus muscle, we identified 114 differentially expressed genes (DEGs), of

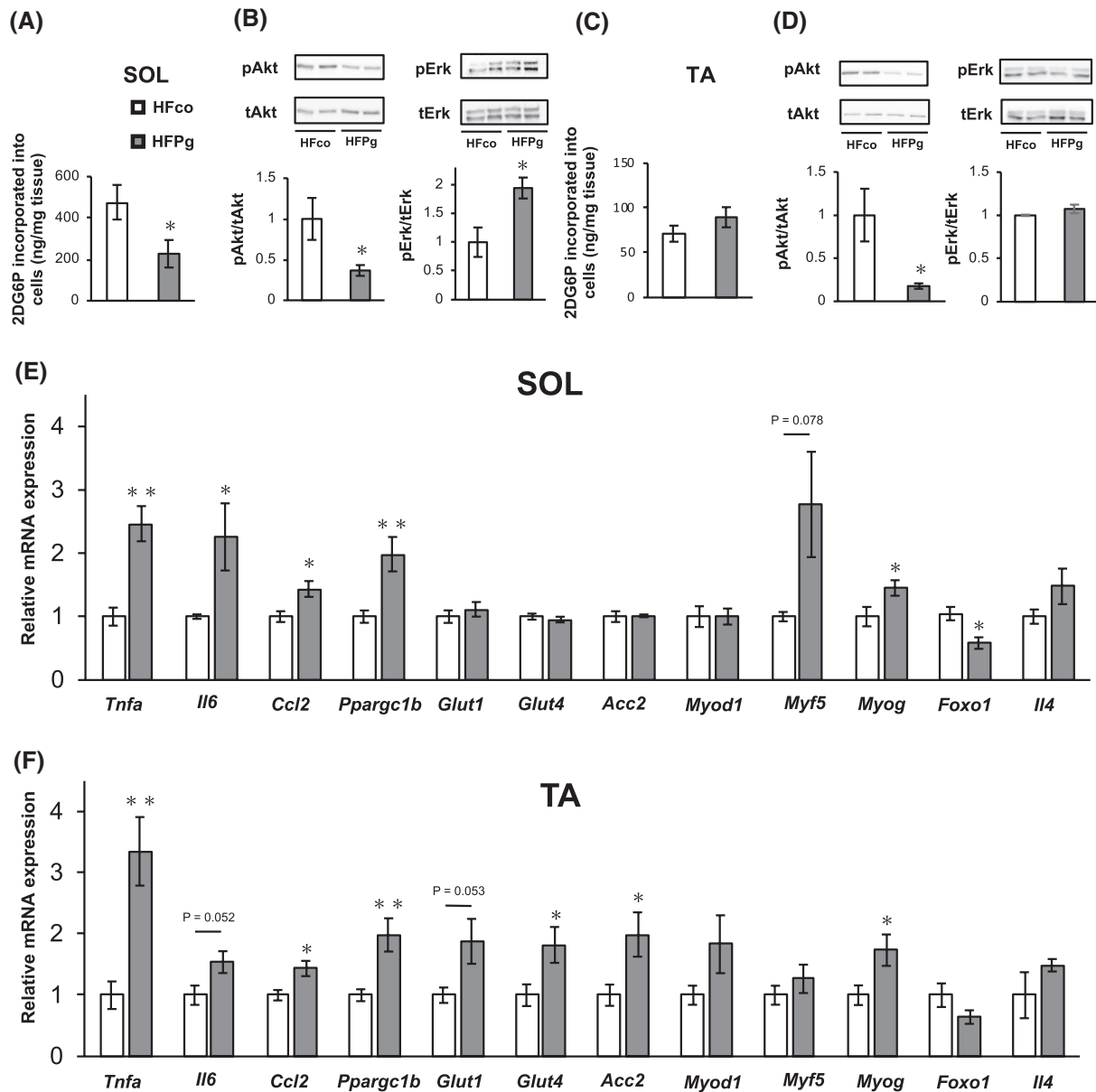


FIGURE 3 Evaluation of 2DG uptake and insulin resistance in skeletal muscle between HFco and HFPg mice ($n = 4-5$). A, 2DG6P incorporation into the soleus muscle between HFco and HFPg mice. B, Western blotting analysis of total Akt, pAkt, total Erk, and pErk expressions in soleus muscle. C, 2DG6P incorporation into the tibialis anterior muscle (TA) between HFco and HFPg mice. D, Western blotting analysis of total AKT, pAKT, total ERK, and pERK expressions in tibialis anterior muscle. mRNA expressions of inflammatory, chemokine, glucose transport, steatosis, and myogenesis-related genes in (E) soleus muscle and (F) tibialis anterior muscle. Relative mRNA expression levels were determined by qPCR and normalized to *I8S* mRNA levels. Data are presented as mean \pm standard error. * $P < .05$ and ** $P < .01$

which 61 were upregulated in HFPg samples (Figure 4A,E). However, only 1 DEG between HFco and HFPg mice was identified in the tibialis anterior muscle (Figure 4B). The gene expression patterns of the soleus muscle in the HFco and HFPg mice differed substantially (Figure 4C), whereas they were not clearly distinct in the tibialis anterior muscle (Figure 4D).

Gene Set Enrichment Analysis (GSEA) was performed using hallmark gene sets to evaluate the differences in mRNA expression levels in the soleus muscles of the HFco and HFPg mice. The gene sets in Table 3 are those with an FDR

q -value < 0.05 . Although we did not observe any downregulated gene sets with an FDR q -value < 0.05 in the soleus muscles of HFPg mice, we observed enrichment of several gene sets, including those related to Interferon- α response, IL2 STAT5 signaling, and IL6 JAK STAT signaling, in HFPg mice. Notably, gene sets related to the TNF α signaling via NF κ B (Figure 5A; normalized enrichment score = 1.82, $q = 0.004$) and inflammatory response (Figure 5B; normalized enrichment score = 1.66, $q = 0.018$) were enriched in the HFPg mice. In addition, the incorporation of 2DG into C2C12 cells was significantly decreased by preincubation for

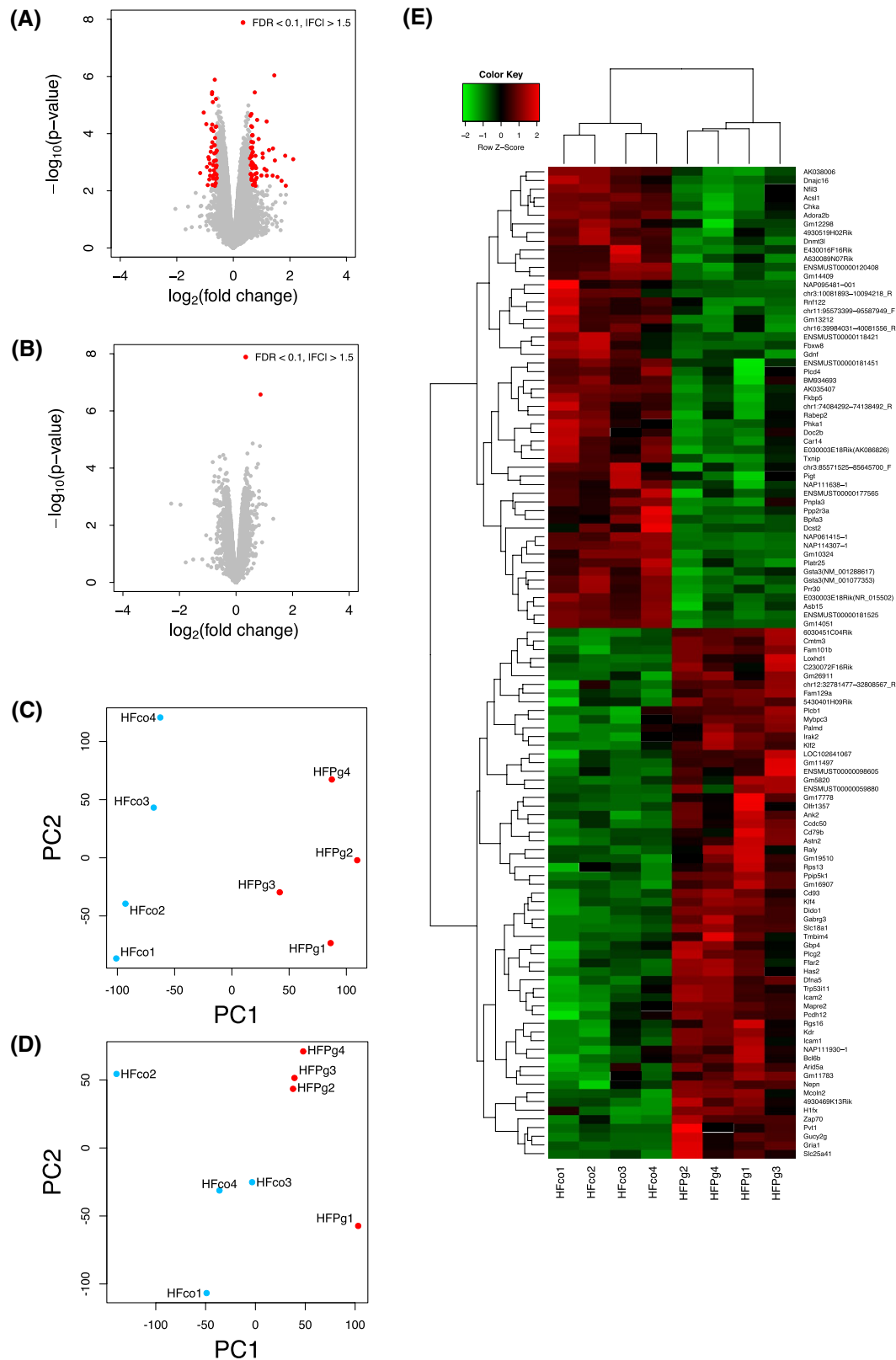


FIGURE 4 Microarray analysis in the soleus (SOL) and tibialis anterior (TA) muscles between HFco and HFPg mice ($n = 4$). Volcano plots of (A) SOL and (B) TA between HFco and HFPg mice at 6 weeks. PCA analysis of (C) SOL and (D) TA between HFco and HFPg mice at 6 weeks after 6 hours fasting. E, Dendrogram and heatmap were constructed based on DEGs in soleus muscle

60 and 180 minutes with TNF- α (Figure 5C). TNF- α treatment for 180 min (0.2, 2, and 20 ng/mL) also decreased 2DG uptake in a dose-dependent manner (Figure 5D).

3.5 | Evaluation of gut microbiome composition based on 16S rRNA gene sequences

A total of 2,770,127 sequence reads was generated by 16S rRNA gene sequencing, corresponding to an average of 197,866.2143 (range: 82,174–337,706) reads per sample. Principal coordinate analysis (PCoA) revealed different microbiome compositions in the HFco and HFPg groups, as determined by ANOSIM (Figure 6A; correlation of $R = .3125$, $P = .061$). No significant differences in the number of OTUs (Figure 6B), Shannon (Figure 6C), and Chao1 (Figure 6D) indices were observed between the HFco and HFPg mice. Relative abundance of the phylum Proteobacteria was significantly higher, and that of the phylum Actinobacteria was significantly lower after *Pg* administration (Figure 6E and Supporting Information S4). At the class level, Coriobacteriia and Erysipelotrichia were represented at a significantly lower level in the HFPg group than in the HFco group, whereas Betaproteobacteria was represented at a significantly higher level (Figure 6F and Supporting Information S5). In addition, we observed significantly lower representation of organisms from order Turicibacterales (Figure 6G and Supporting Information S6), family Turicibacteraceae (Figure 6H and Supporting Information S7), and genus *Turicibacter* (Figure 6I and Supporting Information S8) in HFPg mice. Overall, the microbiome compositions in the guts of HFco and HFPg mice differed based on the ANOSIM

analysis—phylum level: $R = .2917$ and $P = .064$; class level: $R = .3646$ and $P = .03$; order level: $R = .3854$ and $P = .035$; family level: $R = .3125$ and $P = .03$; and genus level: $R = .3646$ and $P = .037$.

On the contrary, relative abundance of the phylum Deferribacteres was significantly higher in NCPg mice compared to NCco mice (Supporting Information S9 and S10). Although PCoA analysis showed separated plotting between NCco and NCPg mice (Supporting Information S9), there was no significant difference in the relative abundance of bacteria at class, order, family, and genus levels between NCco and NCPg mice. The microbiome compositions in the guts of NCco and NCPg mice slightly differed based on the ANOSIM analysis—phylum level: $R = .5556$ and $P = .10$.

3.6 | Network analysis of the gut microbiota

We analyzed co-occurrence relationships in the 16S rRNA profiles of each genus by constructing network structures in which two co-occurring genera were indicated by a node and edge. The values of the clustering coefficients were 0.596 and 0.649 in HFco and HFPg mice, respectively. Focusing on the main networks, we identified 28 and 29 nodes in HFco (Figure 7A) and HFPg (Figure 7B) mice, respectively. Any genus with seven or more co-occurrences with other species and one or more significant co-occurrences in the main networks were classified as interacting core genus. The interacting core genus was altered as there was a decrease in number from 18 to 13, after *Pg* administration. *Turicibacter*, a genus underrepresented after *Pg* administration, was identified as one of the interacting core genera.

TABLE 3 Gene sets showing FDR $q < 0.05$

Gene Set	size	NES	normal P-value	FDR q-Value
Interferon-a response	55	1.93	<.001	0.002
Coagulation	60	1.87	.002	0.002
TNF α signaling via NF κ B	90	1.82	<.001	0.004
IL2 STAT5 signaling	91	1.66	.002	0.016
IL6 JAK STAT signaling	34	1.64	.007	0.016
Inflammatory response	75	1.66	.002	0.018
Estrogen response late	89	1.49	.013	0.047
KRAS signaling	103	1.50	.004	0.049

Abbreviation: NES, normalized enrichment score.

4 | DISCUSSION

In this study, we clearly showed how periodontal bacteria affected metabolic disorders in skeletal muscles. Only the anti-*Pg* IgG antibody titer was significantly and positively correlated with IMAC in MS patients. *Pg* administration altered gut microbiome, especially decreased genus *Turicibacter*. Furthermore, administration of *Pg*-caused adiposity in the soleus muscle, with decreasing insulin signaling and glucose uptake.

Nearly 50% of adults in the United States have periodontitis, including 10% with severe periodontitis.²⁷ Severe periodontitis increases the risk of MS.²⁸ Periodontal diseases are caused predominantly by gram-negative bacteria present in the dental plaque.⁸ In this study, we measured IgG antibody titers, which indicate chronic infection, against three major periodontopathic bacteria in MS patients. In agreement with our previous report,¹⁴ we observed positive correlations between the titers of both anti-*Pg*/anti-*Aa* IgG antibody and HOMA-IR. However, in the present study, we found a

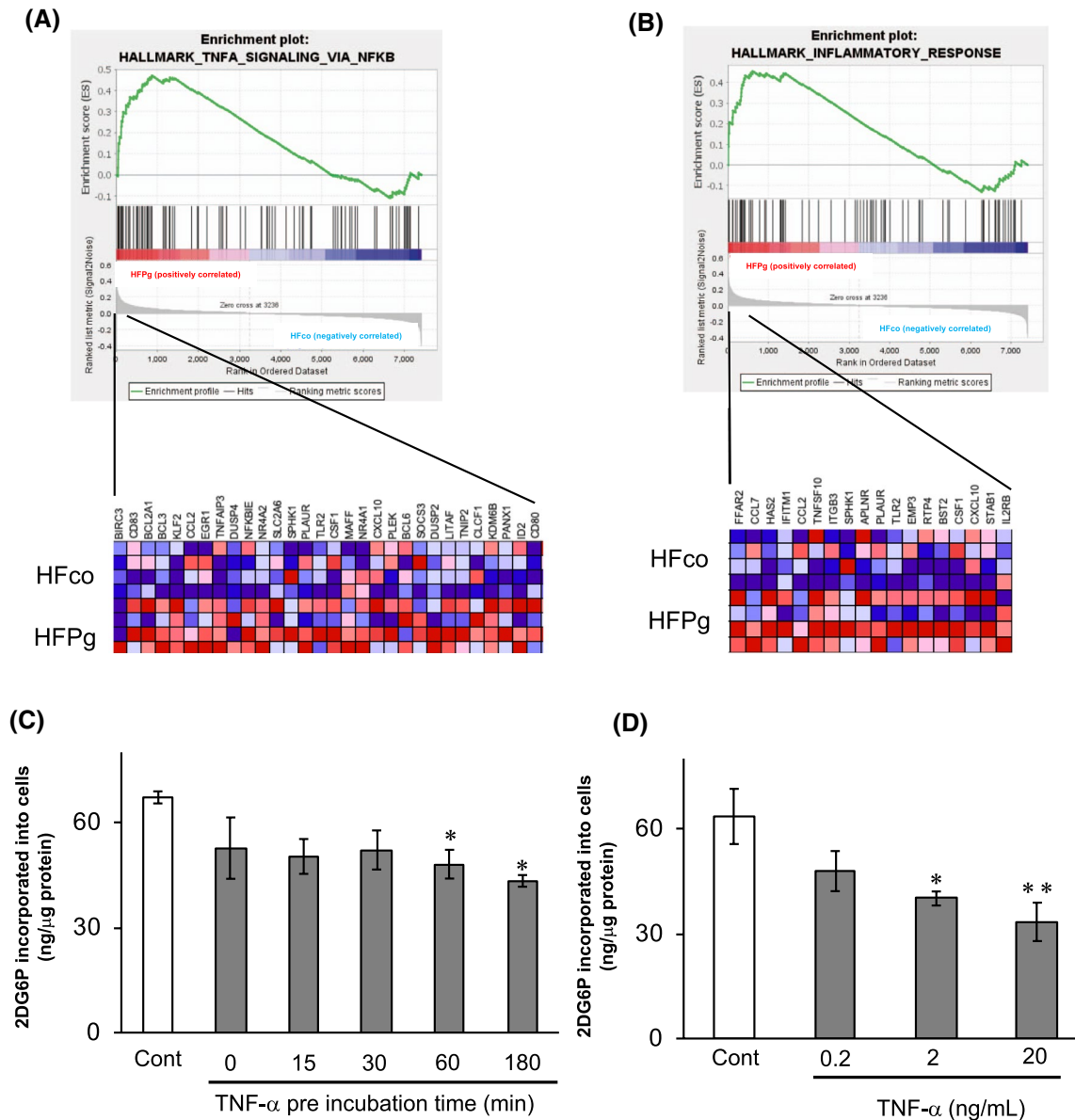


FIGURE 5 GSEA with hallmark gene sets enriched in HFPg mice compared to HFco mice ($n = 4$). Gene set about (A) TNF α signaling via NF κ B and (B) inflammatory response. A heatmap provided illustrating gene expression levels for each gene in the core enrichment subset (blue: low and red: high). C, 2DG6P levels in C2C12 cells after pretreatment with 2 ng/mL TNF- α . (D) 2DG6P level in C2C12 cells after pretreatment with TNF- α (0.2, 2, and 20 ng/mL) for 180 min. Data are presented as mean \pm standard error. * $P < .05$ and ** $P < .01$ compared to control

significant association with the IMAC only for anti-*Pg* IgG antibody titers. *Pg* can impair host defenses by altering the growth and development of the entire microbial community, thereby triggering disruptive changes to their normal homeostatic relationship with the host²⁹; it is considered a major causative pathogen of severe periodontitis.³⁰ A previous study demonstrated a positive correlation between serum anti-*Pg* IgG antibody levels and the oral subgingival distribution of *Pg*.³¹ Furthermore, anti-*Pg* IgG antibody levels of periodontitis patients were significantly higher than those of healthy controls, and the IgG titer against *Pg* was associated with the severity of periodontitis.³² We hypothesized that *Pg* could induce metabolic dysfunction in skeletal muscles.

Skeletal muscles perform nearly 80% of glycogen storage in the body.³³ In this study, only the soleus muscle had lower glucose uptake after *Pg* administration. Skeletal muscles are composed of distinct muscle fiber subtypes—one type of slow-twitch fiber (type I) and three types of fast-twitch fiber (type IIa, type IIx/d, and type IIb)³⁴—defined by their myosin heavy chain isoforms and metabolic activity. The soleus muscle is mainly composed of type I fibers, whereas the tibialis anterior muscle is mainly composed of type II fibers.³⁵ We previously reported that the fibers in the lumbar muscle shifted from type I to type II after feeding mice with a high-fat diet.³⁶ It is possible that the fibers in the soleus muscle change from type I to type II while on the high-fat diet. This

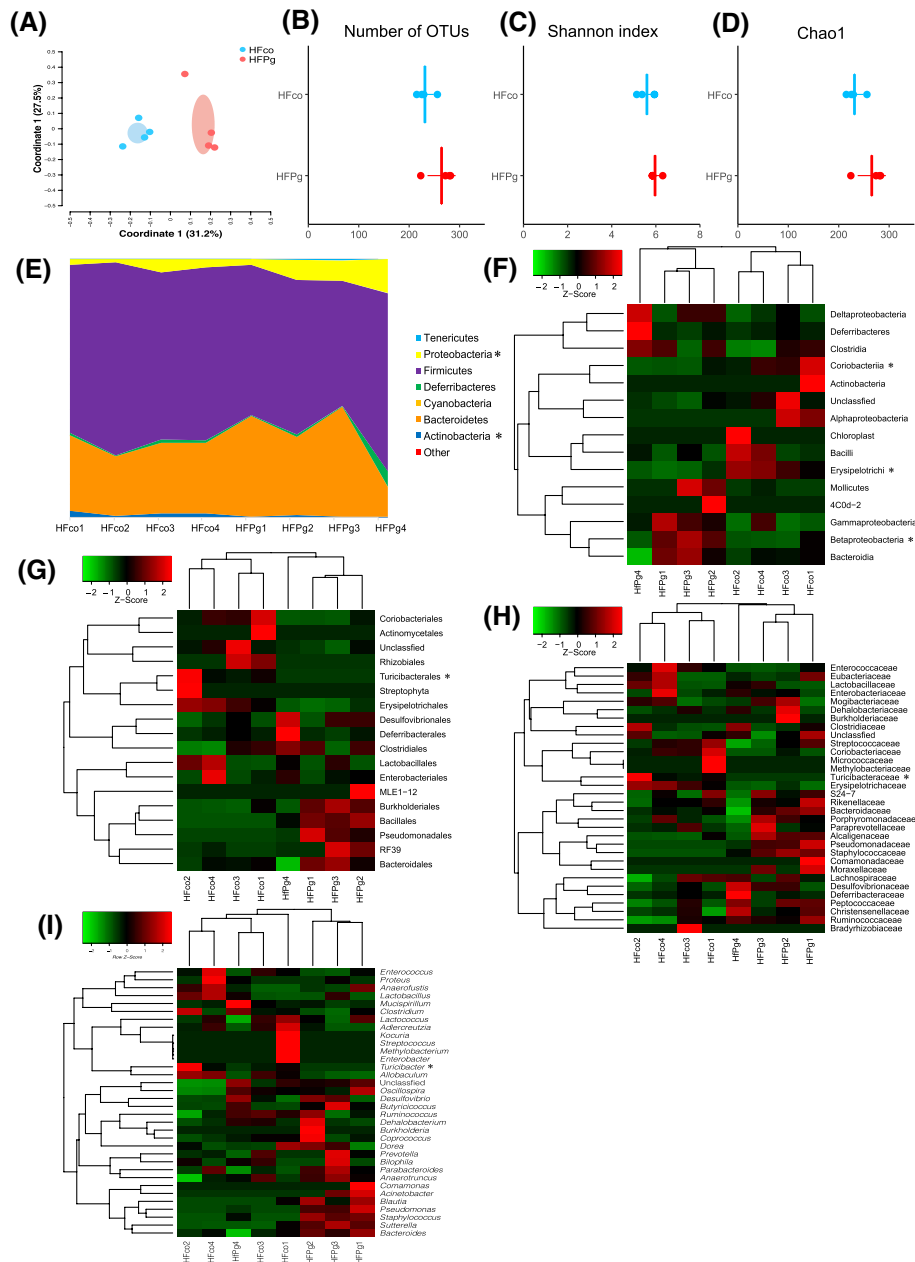


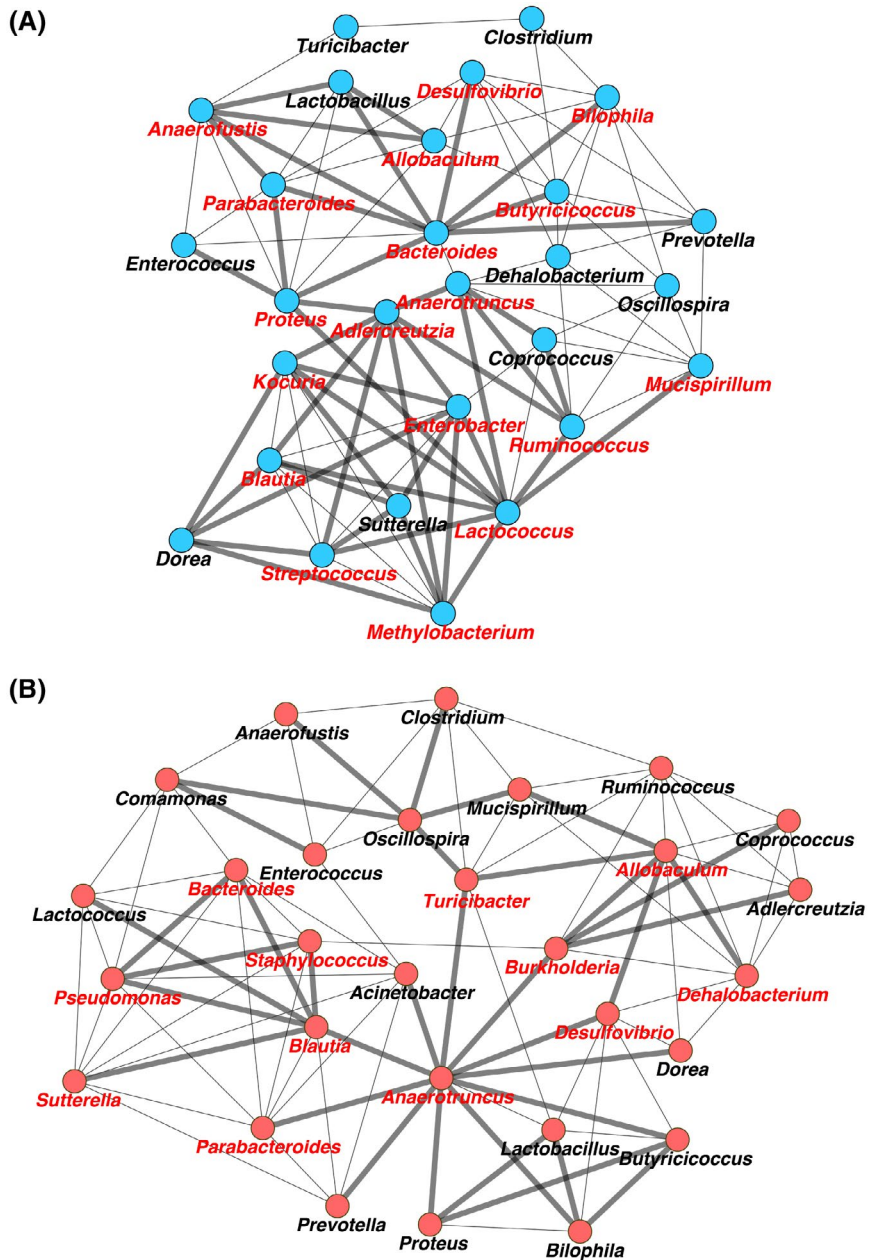
FIGURE 6 Evaluation of gut microbiome compositions based on 16S rRNA gene sequences between HFco and HFPg mice ($n = 4$). A, PCoA analysis, (B) Number of OTUs, (C) Shannon index, (D) Chao1 index. Microbial composition at (E) phylum, (F) class, (G) order, (H) family, and (I) genus level. *Statistically significant difference between HFco and HFPg mice evaluated by analysis of composition of microbiomes (ANCOM) ($q < 0.05$)

transition could explain the difference in the magnitude of the decrease in glucose uptake between the soleus and tibialis anterior muscles. In addition, slow-twitch and fast-twitch muscles have different inflammatory responses after injury.³⁷ This may account for the greater change in gene expression in the soleus vs the tibialis anterior muscles after *Pg* administration that we observed by microarray analysis.

Insulin-stimulated Akt phosphorylation leads to glucose uptake.³⁸ In this study, pAkt was significantly lower in both the soleus and tibialis anterior muscles after *Pg* administration.

However, lower glucose uptake was observed only in the soleus muscle. In addition, increased *Glut1* and *Glut4* expression were observed only in the tibialis anterior muscle. The compensatory increase in *Glut1* and *Glut4* expression in the tibialis anterior muscle could explain its lack of change in glucose uptake. The selective insulin resistance hypothesis posits that elevated levels of glucose and inflammatory cytokines caused by diabetes and insulin resistance selectively inhibit the antiatherogenic action of insulin via the RS/PI3K/Akt pathway, but not the Grb/Shc/MAPK pathway.³⁹

FIGURE 7 Co-occurrence network in the gut microbiome ($n = 4$). Co-occurrence patterns are drawn using a network structure in which each taxon and co-occurrence of genus level was indicated by a node and edge, respectively, for all taxa of genus level pairs with a positive correlation. Taxon pairs with SparCC values ≥ 0.6 are considered as having a co-occurrence relationship with a positive correlation. Interactions with significant co-occurrence network are indicated with bold lines ($P < .05$ and FDR $q < 0.1$). Interacting core genus (showed co-occurrence with other genera ≥ 7 and significant co-occurrence 1 in the main network) is indicated in red text. A, HFco. B, HFPg



However, we observed Erk phosphorylation only in the soleus muscle after *Pg* administration; this may be caused by compensatory changes in response to lower glucose uptake.

Notably, the gene set “TNF α signaling via NF κ B” was enriched in the soleus muscle of HFPg mice. NF κ B, which plays an essential role in inflammation, is related to the development of obesity-induced insulin resistance and MS.⁴⁰ Glucose uptake may be decreased accordingly to increase of *Tnfa* expression and enrichment of inflammatory response and TNF α signaling via NF κ B gene sets in soleus muscle. Our in vitro finding that TNF α impaired glucose uptake in C2C12 cells is consistent with a previous finding in 3T3-L1 cells.⁴¹

There is a close relationship between diabetes and periodontal disease.¹² As the reason why periodontal disease

affects diabetes, some previous reports showed that systemic inflammatory mediators, including TNF α , were increased in patients with severe periodontal disease⁴² and caused insulin resistance.⁴³ In addition, bacteremia originated from the periodontal pocket is also supposed.⁴⁴ In this study, swallowing *Pg* altered the composition of gut microbiome, and *Pg* administered mice showed insulin resistance and impaired glucose tolerance. Swallowing bacteria could also explain the relationship between diabetes and periodontal disease.

In standard diet mice, the relative abundance of the phylum Deferribacteres was significantly higher after *Pg* administration. The phylum Deferribacteres is involved in iron metabolism,⁴⁵ and abnormal iron metabolism was

associated with a greater risk of type 2 diabetes mellitus.⁴⁶ However, no significant difference in phylum Deferribacteres was observed between HFco and HFPg mice. This might be due to the high-fat diet strongly affecting the composition of gut microbiota in mice. In accordance with the alteration of the microbiome that we observed in HFPg mice, a greater relative abundance of phylum Proteobacteria and a lower abundance of phylum Actinobacteria have been observed in obese patients than in healthy subjects.⁴⁷ In particular, we observed that the order Turicibacterales, family Turicibacteraceae, and genus *Turicibacter* were underrepresented in mice treated with oral *Pg*. The abundance of *Turicibacter* correlates with the production of butyric acid,⁴⁸ and an increase in butyrate has been associated with improved insulin sensitivity.⁴⁹ A previous report showed that the muscle mass/body weight ratio was increased in young germ-free mice fed a mixture of the short-chain fatty acids, acetate, propionate, and butyrate when compared to control-fed germ-free mice.⁵⁰ We previously reported that the abundance of *Turicibacter* was decreased upon oral administration of another periodontal bacterium, *A. actinomycetemcomitans*, in mice.¹⁴ These findings suggest that the administration of periodontal bacteria may negatively affect insulin resistance by decreasing the abundance of *Turicibacter* in the gut, thereby decreasing insulin sensitivity.

Interestingly, the microbial network of the gut microbiome was dramatically changed by *Pg* administration. The number of interacting core genus decreased from 18 to 13 after *Pg* administration. In addition, *Turicibacter* was an interacting core genus only in HFPg mice, not in HFco mice. Although genus *Allobaculum* was represented as an interacting core genus both in HFco and HFPg mice, it showed significant co-occurrence with *Turicibacter* only in HFPg mice. The abundance of *Allobaculum* is increased after treatment for dyslipidemia in mice,⁵¹ and mice fed a high-fat diet have a lower abundance of *Allobaculum* in the gut.⁵² Although it did not reach statistical significance, we observed a tendency for a lower abundance of *Allobaculum* in HFPg mice than in HFco mice. This result may also suggest that the effects of *Pg* administration on skeletal muscle dysfunction were caused by a reduction in the abundance of *Turicibacter* and alteration of co-occurrence interactions between *Turicibacter* and other core genera.

Sarcopenia is the progressive loss of muscle mass with increasing age.⁵³ Sarcopenic obesity is characterized by elevated body fat mass combined with reduced muscle mass.⁵⁴ The prevalence of sarcopenic obesity is projected to increase with an increase in the elderly population.⁵⁵ Sarcopenia and sarcopenic obesity cause morbidity,⁵⁶ disability,⁵⁶ and increases in health management costs.⁵⁷ In this study, *Pg* infection-caused symptoms associated with sarcopenic obesity

and metabolic dysfunction in the soleus muscle. Our findings suggest that the prevention and treatment of periodontal disease could contribute to decreasing the incidence of sarcopenic obesity.

In conclusion, infection with the periodontal bacterium *Pg* may be a risk factor for MS and metabolic dysfunction in skeletal muscle. This is the first study to suggest that periodontal bacteria induce insulin resistance and decrease glucose uptake in skeletal muscle by altering the gut microbiota.

ACKNOWLEDGMENTS

This work was supported by JSPS KAKENHI Grant Number JP17K11982 and 20H03863 to SK, JP18K15754 to Hirokazu T., JP19K24062 to NS, JP20J13034 to KW, JP19K18989 to SM, JP19K10221 to Haruka T., and JP18K11016 to AH Grant-in-Aid for Scientific Research at Tokyo Medical and Dental University. This study was supported by Nanken-Kyoten, TMDU. The authors would like to thank Mayumi Tamari, Division of Molecular Genetics, Research Center for Medical Science, The Jikei University School of Medicine, and Toshiyuki Nagasawa, Division of Advanced Clinical Education, School of Dentistry, Health Sciences University of Hokkaido for their kind support, as well as the staff at TMDU's experimental animal center.

CONFLICT OF INTEREST

The authors declare no potential conflicts of interest in this study.

AUTHOR CONTRIBUTIONS

K. Watanabe performed most of the experiments and wrote the 1st draft of the manuscript; S. Katagiri, N. Sasaki, S. Maekawa, R. Komazaki, Y. Ohsugi, H. Tohara, and T. Iwata assisted in some studies and reviewed the manuscript; H. Takahashi, Y. Kitajima, K. Tanaka, Y. Eguchi, and K. Anzai examined subjects and evaluated clinical and biochemical parameters; M. Hatasa and A. Matsuzawa provided expertise on microarray analysis; T. Shiba, K. Komatsu, and T. Hirota provided advice on 16S rRNA sequencing analysis; Y. Maruyama and A. Hattori provided advice on measurement of 2DG uptake using the LC-MS/MS system; S. Katagiri and H. Takahashi designed and supervised all the studies and the writing of the manuscript.

ORCID

Kazuki Watanabe  <https://orcid.org/0000-0003-1860-4358>

Sayaka Katagiri  <https://orcid.org/0000-0002-5765-2742>

Haruka Tohara  <https://orcid.org/0000-0001-5514-6419>

Atsuhiko Hattori  <https://orcid.org/0000-0002-4961-3129>

Takanori Iwata  <https://orcid.org/0000-0002-5461-7298>

REFERENCES

1. Frontera WR, Ochala J. Skeletal muscle: a brief review of structure and function. *Calcif Tissue Int.* 2015;96:183-195.
2. Shadrin IY, Khodabukus A, Bursac N. Striated muscle function, regeneration, and repair. *Cell Mol Life Sci.* 2016;73:4175-4202.
3. Giudice J, Taylor JM. Muscle as a paracrine and endocrine organ. *Curr Opin Pharmacol.* 2017;34:49-55.
4. Meyer C, Dostou JM, Welle SL, Gerich JE. Role of human liver, kidney, and skeletal muscle in postprandial glucose homeostasis. *Am J Physiol Endocrinol Metab.* 2002;282:E419-E427.
5. Zimmet P, Magliano D, Matsuzawa Y, Alberti G, Shaw J. The metabolic syndrome: a global public health problem and a new definition. *J Atheroscler Thromb.* 2005;12:295-300.
6. McCracken E, Monaghan M, Sreenivasan S. Pathophysiology of the metabolic syndrome. *Clin Dermatol.* 2018;36:14-20.
7. Grundy SM, Cleeman JJ, Daniels SR, et al. Diagnosis and management of the metabolic syndrome: an American Heart Association/National Heart, Lung, and Blood Institute Scientific Statement. *Circulation.* 2005;112:2735-2752.
8. Pihlstrom BL, Michalowicz BS, Johnson NW. Periodontal diseases. *Lancet.* 2005;366:1809-1820.
9. Amano A, Nakagawa I, Okahashi N, Hamada N. Variations of *Porphyromonas gingivalis* fimbriae in relation to microbial pathogenesis. *J Periodontol Res.* 2004;39:136-142.
10. Saito T, Shimazaki Y, Sakamoto M. Obesity and periodontitis. *N Engl J Med.* 1998;339:482-483.
11. Martinez-Herrera M, Silvestre-Rangil J, Silvestre FJ. Association between obesity and periodontal disease. A systematic review of epidemiological studies and controlled clinical trials. *Med Oral Patol Oral Cir Bucal.* 2017;22:e708-e715.
12. Preshaw PM, Alba AL, Herrera D, et al. Periodontitis and diabetes: a two-way relationship. *Diabetologia.* 2012;55:21-31.
13. Lamster IB, Pagan M. Periodontal disease and the metabolic syndrome. *Int Dent J.* 2017;67:67-77.
14. Komazaki R, Katagiri S, Takahashi H, et al. Periodontal pathogenic bacteria, *Aggregatibacter actinomycetemcomitans* affect non-alcoholic fatty liver disease by altering gut microbiota and glucose metabolism. *Sci Rep.* 2017;7:13950.
15. Teramoto T, Sasaki J, Ueshima H, et al. Metabolic syndrome. *J Atheroscler Thromb.* 2008;15:1-5.
16. Kitajima Y, Takahashi H, Akiyama T, et al. Supplementation with branched-chain amino acids ameliorates hypoalbuminemia, prevents sarcopenia, and reduces fat accumulation in the skeletal muscles of patients with liver cirrhosis. *J Gastroenterol.* 2018;53:427-437.
17. Udagawa S, Katagiri S, Maekawa S, et al. Effect of *Porphyromonas gingivalis* infection in the placenta and umbilical cord in pregnant mice with low birth weight. *Acta Odontol Scand.* 2018;76:433-441.
18. Sasaki N, Katagiri S, Komazaki R, et al. Endotoxemia by *Porphyromonas gingivalis* injection aggravates non-alcoholic fatty liver disease, disrupts glucose/lipid metabolism, and alters gut microbiota in Mice. *Front Microbiol.* 2018;9:2470.
19. Katagiri S, Park K, Maeda Y, et al. Overexpressing IRS1 in endothelial cells enhances angioblast differentiation and wound healing in diabetes and insulin resistance. *Diabetes.* 2016;65:2760-2771.
20. Toyoda T, An D, Witzak CA, et al. Myo1c regulates glucose uptake in mouse skeletal muscle. *J Biol Chem.* 2011;286:4133-4140.
21. Bolyen E, Rideout JR, Dillon MR, et al. Reproducible, interactive, scalable and extensible microbiome data science using QIIME 2. *Nat Biotechnol.* 2019;37:852-857.
22. Mandal S, Van Treuren W, White RA, Eggesbø M, Knight R, Peddada SD. Analysis of composition of microbiomes: a novel method for studying microbial composition. *Microb Ecol Health Dis.* 2015;26:27663.
23. Friedman J, Alm EJ. Inferring correlation networks from genomic survey data. *PLoS Comput Biol.* 2012;8:e1002687.
24. Shiba T, Watanabe T, Kachi H, et al. Distinct interacting core taxa in co-occurrence networks enable discrimination of polymicrobial oral diseases with similar symptoms. *Sci Rep.* 2016;6:30997.
25. Subramanian A, Tamayo P, Mootha VK, et al. Gene set enrichment analysis: a knowledge-based approach for interpreting genome-wide expression profiles. *Proc Natl Acad Sci U S A.* 2005;102:15545-15550.
26. Pajak B, Siwiak E, Sołtyka M, et al. 2-Deoxy-d-glucose and its analogs: from diagnostic to therapeutic agents. *Int J Mol Sci.* 2019;21:234.
27. Eke PI, Dye BA, Wei L, et al. Update on prevalence of periodontitis in adults in the United States: NHANES 2009 to 2012. *J Periodontol.* 2015;86:611-622.
28. Kim OS, Shin MH, Kweon SS, et al. The severity of periodontitis and metabolic syndrome in Korean population: The Dong-gu study. *J Periodontol Res.* 2018;53:362-368.
29. Hajishengallis G, Liang S, Payne MA, et al. Low-abundance biofilm species orchestrates inflammatory periodontal disease through the commensal microbiota and complement. *Cell Host Microbe.* 2011;10:497-506.
30. Mysak J, Podzimek S, Sommerova P, et al. *Porphyromonas gingivalis*: major periodontopathic pathogen overview. *J Immunol Res.* 2014;2014:476068.
31. Kojima T, Yano K, Ishikawa I. Relationship between serum antibody levels and subgingival colonization of *Porphyromonas gingivalis* in patients with various types of periodontitis. *J Periodontol.* 1997;68:618-625.
32. Kudo C, Naruishi K, Maeda H, et al. Assessment of the plasma/serum IgG test to screen for periodontitis. *J Dent Res.* 2012;91:1190-1195.
33. Jensen J, Rustad PI, Kolnes AJ, Lai Y-C. The role of skeletal muscle glycogen breakdown for regulation of insulin sensitivity by exercise. *Front Physiol.* 2011;2:112.
34. Schiaffino S, Reggiani C. Fiber types in mammalian skeletal muscles. *Physiol Rev.* 2011;91:1447-1531.
35. Kammoun M, Cassar-Malek I, Meunier B, Picard B. A simplified immunohistochemical classification of skeletal muscle fibres in mouse. *Eur J Histochem.* 2014;58:2254.
36. Hua N, Takahashi H, Yee GM, et al. Influence of muscle fiber type composition on early fat accumulation under high-fat diet challenge. *PLoS ONE.* 2017;12:e0182430.
37. Zimowska M, Kasprzycka P, Bocian K, et al. Inflammatory response during slow- and fast-twitch muscle regeneration. *Muscle Nerve.* 2017;55:400-409.
38. Dean DJ, Brozinick JT, Cushman SW, Cartee GD. Calorie restriction increases cell surface GLUT-4 in insulin-stimulated skeletal muscle. *Am J Physiol.* 1998;275:E957-E964.
39. King GL, Park K, Li Q. selective insulin resistance and the development of cardiovascular diseases in diabetes: The 2015 Edwin Bierman Award Lecture. *Diabetes.* 2016;65:1462-1471.

40. Baker RG, Hayden MS, Ghosh S. NF- κ B, inflammation, and metabolic disease. *Cell Metab.* 2011;13:11-22.
41. Iwata M, Haruta T, Usui I, et al. Pioglitazone ameliorates tumor necrosis factor- α -induced insulin resistance by a mechanism independent of adipogenic activity of peroxisome proliferator-activated receptor- γ . *Diabetes.* 2001;50:1083-1092.
42. Nishimura F, Iwamoto Y, Mineshiba J, Shimizu A, Soga Y, Murayama Y. Periodontal disease and diabetes mellitus: the role of tumor necrosis factor- α in a 2-way relationship. *J Periodontol.* 2003;74:97-102.
43. Sun W-L, Chen L-L, Zhang S-Z, Wu Y-M, Ren Y-Z, Qin G-M. Inflammatory cytokines, adiponectin, insulin resistance and metabolic control after periodontal intervention in patients with type 2 diabetes and chronic periodontitis. *Intern Med.* 2011;50:1569-1574.
44. Page RC. The pathobiology of periodontal diseases may affect systemic diseases: inversion of a paradigm. *Ann Periodontol.* 1998;3:108-120.
45. Li Y, Luan Y, Yue X, et al. Effects of *Codonopsis bulleyana* forest ex diels on *Deferribacteres* in constipation predominant intestine tumor: Differential analysis. *Saudi J Biol Sci.* 2019;26:395-401.
46. Fernández-Real JM, McClain D, Manco M. Mechanisms linking glucose homeostasis and iron metabolism toward the onset and progression of type 2 diabetes. *Diabetes Care.* 2015;38:2169.
47. Zhu L, Baker SS, Gill C, et al. Characterization of gut microbiomes in nonalcoholic steatohepatitis (NASH) patients: a connection between endogenous alcohol and NASH. *Hepatology.* 2013;57:601-609.
48. Zhong Y, Nyman M, Fåk F. Modulation of gut microbiota in rats fed high-fat diets by processing whole-grain barley to barley malt. *Mol Nutr Food Res.* 2015;59:2066-2076.
49. Vrieze A, Van Nood E, Holleman F, et al. Transfer of intestinal microbiota from lean donors increases insulin sensitivity in individuals with metabolic syndrome. *Gastroenterology.* 2012;143:913-916.e917.
50. Lahiri S, Kim H, Garcia-Perez I, et al. The gut microbiota influences skeletal muscle mass and function in mice. *Sci Transl Med.* 2019;11:eaan5662.
51. Raza GS, Putaala H, Hibberd AA, et al. Polydextrose changes the gut microbiome and attenuates fasting triglyceride and cholesterol levels in Western diet fed mice. *Sci Rep.* 2017;7:5294.
52. Everard A, Lazarevic V, Gaïa N, et al. Microbiome of prebiotic-treated mice reveals novel targets involved in host response during obesity. *ISME J.* 2014;8:2116-2130.
53. Rosenberg IH. Sarcopenia: origins and clinical relevance. *J Nutr.* 1997;127:990S-991S.
54. Zoico E, Di Francesco V, Guralnik JM, et al. Physical disability and muscular strength in relation to obesity and different body composition indexes in a sample of healthy elderly women. *Int J Obes Relat Metab Disord.* 2004;28:234-241.
55. Batsis JA, Villareal DT. Sarcopenic obesity in older adults: aetiology, epidemiology and treatment strategies. *Nat Rev Endocrinol.* 2018;14:513-537.
56. Janssen I, Heymsfield SB, Ross R. Low relative skeletal muscle mass (sarcopenia) in older persons is associated with functional impairment and physical disability. *J Am Geriatr Soc.* 2002;50:889-896.
57. Janssen I, Shepard DS, Katzmarzyk PT, Roubenoff R. The health-care costs of sarcopenia in the United States. *J Am Geriatr Soc.* 2004;52:80-85.

SUPPORTING INFORMATION

Additional Supporting Information may be found online in the Supporting Information section.

How to cite this article: Watanabe K, Katagiri S, Takahashi H, et al. *Porphyromonas gingivalis* impairs glucose uptake in skeletal muscle associated with altering gut microbiota. *The FASEB Journal.* 2020;00:1-16. <https://doi.org/10.1096/fj.202001158R>